Pyrene-Capped Conjugated Amorphous Starbursts: Synthesis, Characterization, and Stable Lasing Properties in Ambient Atmosphere

Weidong Xu, Jianpeng Yi, Wen-Yong Lai, Li Zhao, Qi Zhang, Wenbo Hu, Xin-Wen Zhang, Yi Jiang, Ling Liu, and Wei Huang**

A family of trigonal starburst conjugated molecules (TrFPy, TrFPy, and TrF2Py) composed of a truxene core and pyrene cappers with various bridge lengths is synthesized and characterized. The incorporation of pyrene cappers successfully depress the crystallization tendency, resulting in enhanced glassy temperature and improved morphological stability of the thin films. The high photoluminescence yield in neat films and excellent thermal stability render these pyrene-capped starbursts promising lasing optical gain media. Low amplified spontaneous emission (ASE) thresholds (E_{th}^{ASE}) of 180 nJ pulse^{-1} and 101 nJ pulse^{-1} were recorded for TrFPy and TrF2Py, respectively. One dimensional distributed feedback (1D DFB) lasers demonstrated lasing threshold of 9.3 kW/cm^2 and 7.3 kW/cm^2 for TrFPy (at 457 nm) and TrF2Py lasers (at 451 nm), respectively. The ASE performance of TrFPy and TrF2Py in an ambient condition was recorded with various annealing temperature (from 80 to 250 °C, 10 min). Surprisingly, TrFPy exhibited excellent ASE stability in an ambient condition, which is still detectable even after annealing at 250 °C for 10 min. The results suggest the pyrene-capped molecular design strategy is positive on improving the optical gain stability and meanwhile maintaining excellent lasing properties.

1. Introduction

Solution-processed organic semiconductor emitters are promising broadly tunable coherent sources which have the benefits of low-cost processing, light weight physical characteristics, tunable optoelectronic properties, and the attractive possibility of direct integration into flexible substrates. In contrast to the widely utilized lasing dyes, one of the most attractive properties is that organic semiconductors possess the possibilities of being pumped directly by electrical injection.[1–4] Although numerous solution-processed emitters have been demonstrated in organic light emitting diodes (OLEDs), it should be noted that not all materials that show good performance in OLEDs exhibit efficient optical gain at low pump thresholds. Unrevealing the structure-function relationships is a vital research task with the aim to shed light on rational design and development of high-performance optical gain materials. Particularly, to address the challenge of electrically pumped organic laser diodes, researchers have devoted considerable efforts to realize large stimulated emission cross-sections (σ_e), low lasing thresholds, high carrier mobility, and excellent power-conversion efficiencies.[5–9] Nevertheless, the development of efficient optical gain materials is still highly demanded.

From a fundamental viewpoint, molecules with well-defined structures are critical for understanding the structural properties and functions. This rule also applies to the study of the lasing and/or spontaneous emission property of organic semiconductors. Good solution processability is one of the attractive prerequisites, which make organic semiconductor lasers suffer little from the concentration quenching that plagues typical dye-doped organic lasers. In our previous contribution, we have explored a novel series of monodisperse starburst conjugated macromolecules based on truxene or triazatruxene cores with three or six oligofluorene arms.[10–14] Promising

W. Xu, J. Yi, Prof. W.-Y. Lai, L. Zhao, Q. Zhang, W. Hu, X.-W. Zhang, Y. Jiang, L. Liu, Prof. W. Huang
Key Laboratory for Organic Electronics and Information Displays (KLOEID)
Institute of Advanced Materials (IAM)
Jiangsu National Synergetic Innovation Center for Advanced Materials (SICAM)
Nanjing University of Posts and Telecommunications
9 Wenyuan Road, Nanjing 210023, China
E-mail: iamwylai@njupt.edu.cn; wei-huang@njtech.edu.cn

Prof. W.-Y. Lai, Prof. W. Huang
Key Laboratory of Flexible Electronics (KLOFE) and Institute of Advanced Materials (IAM)
Jiangsu National Synergetic Innovation Center for Advanced Materials (SICAM)
Nanjing Tech University (NanjingTech)
30 South Puzhu Road, Nanjing 211816, China

DOI: 10.1002/adfm.201501337

electroluminescence, optical gain, and lasing performance have been achieved. Well-defined chemical structures, high purity, excellent reproducibility, good solution processability, and general superior optoelectronic properties are the main advantages of these monodiperse star-shaped multiarmed materials.[10–14] These studies have enabled us to systematically investigate the relationships between the arm length, arm number, core type and the resulting lasing and electroluminence properties. Furthermore, an extremely low-threshold lasing has been demonstrated by a 1D distributed feedback (DFB) laser with a six-armed starburst material as gain media (T3, 1.3 μJ cm^{-2}).[12]

From a practical standpoint, high environmental stability is strongly demanded in organic lasers since the gain media have to be exposed under high-fluence pumped sources. For achieving electrically pumped organic laser diodes, a much higher current density is necessary in comparison to those typical OLEDs. This requires that the laser gain media should possess not only high carrier mobility but also good thermal and optical stability. The widely investigated polyfluorene, e.g., poly(9,9-dioctylfluorene) (PFO), shows a continuous increase in amplified spontaneous emission (ASE) threshold by annealing from room temperature up to 130 °C (0.32 μJ to 2.0 μJ $pulse^{-1}$), and the ASE tends to be undetectable with the annealing temperature above 150 °C, as suggested by Sim et al. [15] Pyrene derivatives have attracted much recent interest due to their high photoluminescence quantum yields (PLQYs), high charge carrier mobility, and excellent thermal stability.[16] Incorporating with other highly emissive building blocks, such as fluorene and anthracene units, pyrene derivatives have been demonstrated as one of the most promising candidates for organic lasing applications.[11] In contrast to the fluorene-based materials that commonly show a poor spectral stability, the outstanding thermal stability for pyrene derivatives is rather attractive.[17] However, planar pyrene molecules tend to form π aggregates/excimers in the solid state, resulting in redshifted aggregates/excimers emission with reduced fluorescence efficiency.[17–23] In order to address these issues, many new materials with hindered structures have been explored and investigated, such as polypyrene molecules,[24] tetraarylpyrene molecules,[17] pyrene–fluorene[25–27] and pyrene–carbazole systems.[28,29] Generally, it is essential to integrate either large bulky groups or multisubstituted rigid moieties to suppress aggregates and excimers. We have recently developed a series of monodisperse multiarmed starbursts with pyrene as the core and oligofluorenes as the arms.[11,17] Such a novel molecular design has been proven to be effective to restrain the aggregation tendency of pyrene units, resulting in not only excellent electroluminescence performance and extremely low-threshold organic lasing, but also improved ASE stability in comparison with those of linear polyfluorenes. Moreover, a modest increase in ASE thresholds with increasing the annealing temperature has been found in N_2-filled atmosphere.[11]

In this contribution, we report the design, synthesis, and optical gain properties of a series of new trigonal starburst conjugated molecules with a truxene core end-capped with pyrene moieties (TrPy, TrFPy, and TrF2Py). Pyrene units were incorporated as the end functional groups and the length of oligofluoene bridges was varied with the aim to provide a set of model samples to reveal the influence of intramolecular charge transfer between the core and the end cappers, and to understand the impact of the photoelectric property variation on the lasing properties. The relationships between their morphology, thermal stability, and corresponding ASE stability in an ambient condition were systematically investigated, which suggests the pyrene-capped molecular design strategy is positive on improving the optical gain stability. Consequently, promising low-threshold and stable lasing properties have been achieved with 1D DFB structures.

2. Results and Discussion

2.1. Synthesis and Characterization

The synthetic routes toward the pyrene-capped starbursts are shown in **Scheme 1**. The key step for the synthesis involves microwave-assisted Pd-mediated Suzuki cross-coupling reaction of 1-bromopyrene or pyrene-capped oligofluorene with 2,7,12-tri-(4′,4′,5′,5′-tetramethyl-1′,3′,2′-dioxaborolane)-hexaethyltruxene. The Suzuki cross-coupling reaction with $Pd(PPh_3)_4$, K_2CO_3, and tetrabutylammonium bromide (TBAB) as catalyst under microwave irradiation (CEM system) for 30 min at 150 °C afforded target compounds in 70%–90% yields. The well-defined structures and chemical purities of the intermediates and the final starbursts have been adequately verified by ^1H and ^{13}C NMR spectroscopy and MALDI-TOF mass spectrometry.

2.2. Photophysical Properties

Figure 1 shows the normalized UV–vis absorption and photoluminescence (PL) spectra for dilute THF solutions (Figure 1a) and spin-coated thin films (Figure 1b) of the starbursts. The normalized UV–vis absorption exhibited a peak at λ_{abs} = 359 nm for TrPy, 362 nm for TrFPy, and 372 nm for TrF2Py, respectively. Slight bathochromic shifts to 368 nm for TrPy, 369 nm for TrFPy, and 375 nm for TrF2Py were observed for the thin film absorption spectra, consistent with denser packing and extended conjugation in the solid states. The corresponding maximum absorption coefficient (α_{max}) were 8.1×10^4, 10.4×10^4, and 10.8×10^4 cm^{-1} for TrPy, TrFPy, and TrF2Py, respectively. The solution PL emission bands of all the starburst compounds showed a 0–0 emission band peak at around 417–418 nm. For TrFPy and TrF2Py in film states, the 0–1 emission peaked at λ_{em} = 451 and 449 nm, respectively, with a 0–0 shoulder at around 427 nm. For TrPy, a broadened and redshifted PL band was observed with a peak at 475 nm in film states, which indicated that the planar pyrene unit directly attached to the truxene core was not effective to circumvent the aggregation tendency, resulting in an obvious emission band from aggregates.

The PLQYs of the compounds in film states were measured by an integrating sphere with λ_{abs} in film states as the excitation wavelength. The PLQY increased with the increment of oligofluorene bridge lengths from 35.7% for TrPy, 56.2% for TrFPy to 60.1% for TrF2Py. The PLQY for the starbursts TrFPy and TrF2Py became close, suggesting that the incorporation of one fluorene

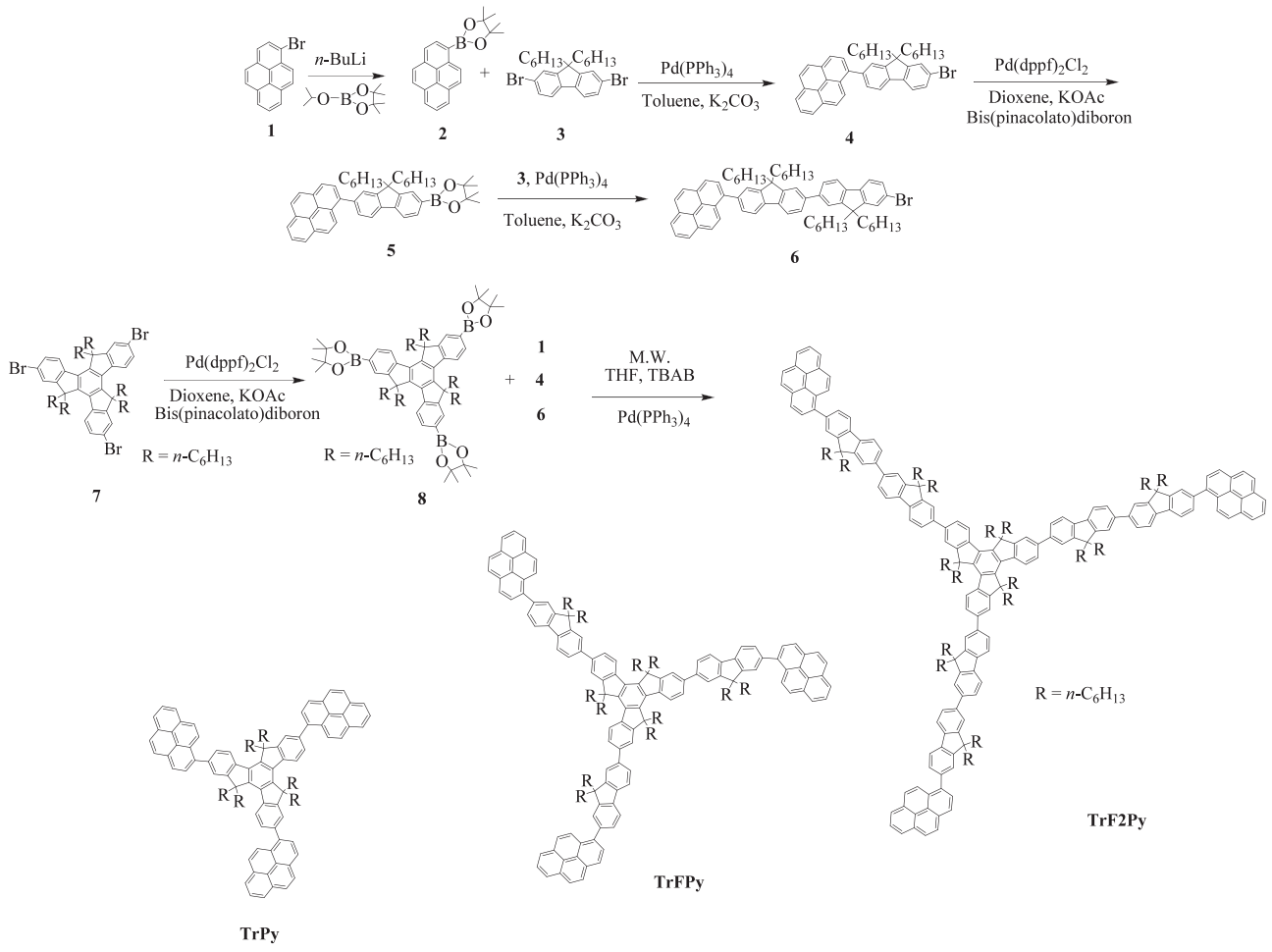

Scheme 1. Synthetic routes toward pyrene-capped starbursts.

unit as the bridge was effective to depress the intramolecular interactions. This was also supported by the observation from the solid-state transient PL measurements. The PL decay transients were plotted as shown in **Figure 2**, which was measured from 60 nm thick films of each compound with 1 MHz, 85 ps pulse excitation. The film of TrPy showed a tri-exponential decay with an initial fast component with a lifetime of $\tau_1 = 0.84$ ns (15.6%), a second fast component with a lifetime of $\tau_2 = 4.84$ ns (43.2%), and a third longer component with a lifetime of $\tau_3 = 15.47$ ns (41.2%). The longest lifetime (τ_3) was probably attributed to the excited-state excimers of the rigid pyrene substituents. In contrast, TrFPy and TrF2Py films showed only two exponential component decays with a fast component at τ_1(TrFPy) = 0.68 ns (67.8%), τ_1 (TrF2Py) = 0.66 ns (71.9%), and a longer component

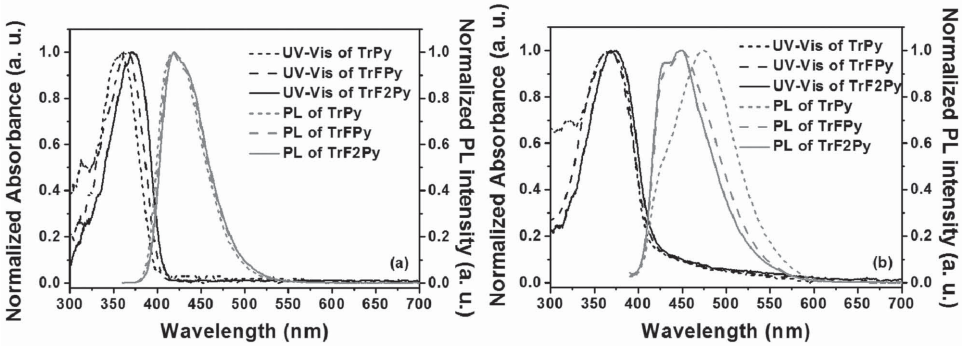

Figure 1. a) UV–vis absorption and PL spectra of TrPy, TrFPy, and TrF2Py in dilute THF solutions and b) in the films spin-cast on quartz from a toluene solution.

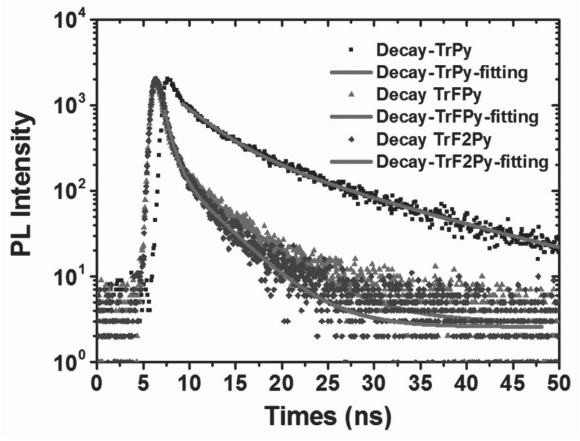

Figure 2. Normalized PL decay transients for TrPy (squares), TrFPy (circles), and TrF2Py (triangles) in the film states (the excitation wavelength is 375 nm).

at τ_2(TrFPy) = 5.05 ns (32.2%), τ_2 (TrF2Py) = 3.05 ns (28.1%), respectively. The prolonged relaxation (τ_2) was ascribed to exciton migration from the truxene core or oligofluorene units to pyrene cappers, which was typically observed in solid states.[30] The radiative lifetime (τ_R) was determined by decay time and PLQY. For TrPy, a long radiative lifetime of 24.08 ns was recorded. The radiative lifetimes of these starbursts decreased with the increment of the arm length. For TrFPy and TrF2Py, the radiative lifetimes were determined as 3.72 and 2.50 ns, respectively. All the optical properties are summarized in **Table 1**.

2.3. Thermal Properties and Morphologies

The thermal properties of trigonal materials were investigated by thermal gravimetric analysis (TGA) and differential scanning calorimetry (DSC) in N_2 atmosphere. The results are shown in **Figure 3**. All these compounds were thermally stable with 5% weight loss temperatures (T_d) of 403 °C for TrPy, 402 °C for TrFPy, and 385 °C for TrF2Py, respectively. Distinct glass transition temperatures (T_g) were observed at 131 °C for TrPy and 168 °C for TrFPy. For TrF2Py, no obvious T_g was found within the heating scans from room temperature to 280 °C (Figure 3, inset). The T_g value of trigonal materials increased obviously with the increment of fluorene units at each bridge from TrPy, TrFPy to TrF2Py, resulting from the increased molecular weight or the enhanced steric hindrance by increasing the arm length.[31] In contrast to previously reported trigonal truxene-cored starburst molecules (T1–T4) with only oligofluorene arms, the T_g values have been enhanced significantly (from T_g = 63 °C for T1 to 116 °C for T4).[13,32] It is implied that the presence of pyrene end-cappers can effectively improve the rigidity of the molecular backbone and limit the crystallization and induce the formation of an amorphous morphology, which in turn improves the thermal and morphological stability of the films.

Atomic force microscopy (AFM) measurements were conducted to understand the film-forming ability. The results were recorded from the pristine films of TrPy, TrFPy, and TrF2Py on quartz, as shown in **Figure 4**a–c, respectively. The pristine TrPy film showed an extremely rough surface with a root-mean-square (rms) roughness of 6.31 nm. Generally, such poor film-forming ability is not desirable for organic semiconductor devices. In contrast, the films of TrFPy and TrF2Py exhibited a smooth and uniform surface with the rms roughness of 0.285 and 0.268 nm, respectively. These results suggested that the increase of arm length of the starbursts could effectively improve the solubility, and therefore enhance their film-forming ability. Figure 4d–f presents a set of fluorescence optical microscope (FOM) images of the same films after thermal annealing at 150 °C for 10 min in ambient condition. Different from the uniform surface of TrF2Py, the annealed TrPy and TrFPy films exhibited micrometer-sized features caused by their relatively low T_g. This result is consistent with their DSC measurements. The good film-forming ability and thermal stability for TrF2Py is highly attractive for lasing.

2.4. Electronic and Electroluminescent Properties

Density functional theory calculations of the starburst compounds were carried out using a suite of Gaussian 03 program in order to understand their electronic properties at the molecular level. The nonlocal density functional of B3LYP with 6-31G(d) basis set was used for the calculation. The optimized structures and the orbital distributions of HOMO and LUMO energy levels of the starbursts are shown in Figure S2 and Table S1 (Supporting Information), respectively. The excited electrons are polarized from the truxene core to pyrene-capped units through the oligofluorene bridge, which indicates that the pyrene units are more likely to accept electrons. It is consistent with the transient PL results that these materials show a long lifetime components (τ_2) around 3–5 ns in neat films. Slight variation of calculated energy levels is found, implying a weak influence for the pyrene cappers on the electronic properties of the molecules. The electrochemical properties of the starburst materials were further

Table 1. Photophysical and electrochemical properties of TrPy, TrFPy, and TrF2Py.

Compound	λ_{abs} [nm] (solution)[a)]	λ_{PL} [nm] (solution) [a)]	λ_{abs} [nm] (film)[b)]	λ_{PL} [nm] (film)[b)]	α_{max} [10^4 cm^{-1}][b)]	PLQY [%][b,c)]	Decay time [ns] [b)]	Radiative lifetime [ns][d)]
TrPy	359	418	368	475	8.1	35.7	0.84 (15.6%), 4.84 (43.2%), 15.47 (41.2%)	24.08
TrFPy	362	417	369	451	10.4	56.2	0.68 (67.8%), 5.05 (32.2%)	3.72
TrF2Py	372	417	375	449	10.8	60.1	0.66 (71.9%), 3.65 (28.1%)	2.50

[a)] ≈5×10^{-7} mol L^{-1} in THF; [b)]PLQY of spin-coated films measured in an integrating sphere; [c)]Prepared by spin-coating at 1200 rpm in toluene (15 mg mL^{-1}). The excitation wavelength is 370 nm. d)Calculated by the equation of $\tau_R = \tau$/PLQY.

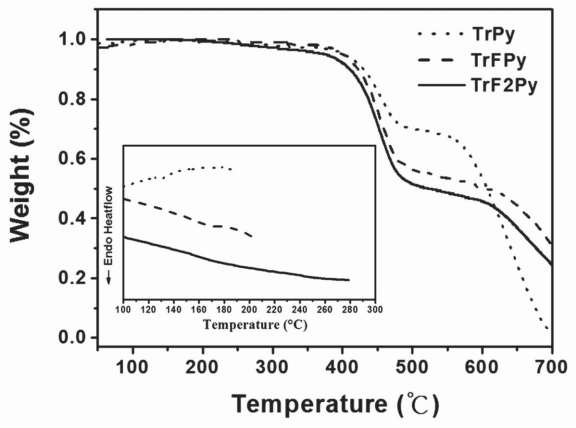

Figure 3. TGA thermograms and DSC traces (inset) of the materials recorded at a heating rate of 10 °C min^{-1}.

investigated by cyclic voltammetry. As shown in Figure S3 and Table S1 (Supporting Information), all the molecules showed similar HOMO levels at around –5.79 to –5.80 eV, indicating p-type characteristics of these materials. The LUMO levels of the starbursts raised slightly from –2.51 eV for TrPy to –2.45 eV for TrFPy and –2.28 eV for TrF2Py, demonstrating the influence of increasing the arm length. To further investigate their electroluminescence properties of these novel starburst materials, and especially their color stability under electrical bias, solution-processed OLEDs with the configuration of ITO/PEDOT:PSS/Emissive Layer/LiF/Al were fabricated. The EL spectra of TrFPy and TrF2Py based devices are shown in Figure S1 (Supporting Information). Because of the poor film-forming ability of TrPy, no good EL performance was recorded. In contrast, both TrFPy and TrF2Py-based OLEDs showed good EL spectral stability with the operating voltage up to 8 V.

2.5. Amplified Spontaneous Emission (ASE) Properties

The ASE properties of TrFPy and TrF2Py in neat films were measured by an Nd:YAG laser (a repetition rate of 10 Hz, a pulse duration of 12 ns) with the pumped source at their maximum absorption wavelength, and the surface emission was collected and analyzed with a fiber-coupled spectrograph and charge-coupled device (CCD) detector. The lowest ASE thresholds (E_{th}^{ASE}) for the TrFPy and TrF2Py films with optimized thickness are 180 nJ pulse $^{-1}$ (11.2 μJ cm^{-2}, peaked at 449 nm) and 105 nJ pulse^{-1} (6.3 μJ cm^{-2}, peaked at 445 nm), respectively. As shown in **Figure 5**b, by controlling the TrF2Py film thickness, we can access lasing wavelengths across a 13 nm spectral window (433–445 nm). It is noted that the ASE phenomenon is even detectable in an ultrathin film of 25 nm, with an increased E_{th}^{ASE} of 356 nJ pulse^{-1} (22.3 μJ cm^{-2}). The 1D DFB lasers based on TrFPy and TrF2Py were fabricated by spin-coated thin films on top of the DFB gratings which were obtained by the method of nanoimprint lithography (NIL). The fill factor of the gratings was 50%, and the periods we chose were 280, 290, and 300 nm. The pulse beam of the frequency-tripled Nd:YAG pulse laser (with the pump wavelength at 355 nm, a repetition rate of 10 Hz, a pulse duration of 5 ns) was used as the pump source, which was focused into a circle-shaped spot with a diameter of 681 μm. As shown in **Figure 6**a, two transitions of the slopes were observed by increasing the pump energy density, indicating lasing threshold of 9.3 kW cm^{-2} for TrFPy (120 nm) with the output wavelength peaked at 457 nm and 7.3 kW cm^{-2} for TrF2Py (108 nm) with the output wavelength peaked at 451 nm, respectively. By regulating the periods of the gratings, the lasing wavelength can be tuned across a spectral window of 17 nm from 442 to 451 nm with the FWHM of 0.2 nm for TrFPy, as depicted in Figure 6b.

The ASE characteristics of TrFPy and TrF2Py were monitored as a function of annealing temperatures (from 80 to 250 °C) to assess the corresponding thermal stability of the gain properties.[33] The measurements were conducted in an ambient condition with room temperature of 20 °C and the humidity of 30%. After cooling back to room temperature fast, standard stripe-pumped ASE measurements were performed. It is worthwhile to mention that the excitation stripe is moved to a fresh location on the films for each successive measurement to prevent annealing effects from photodegradation. The increased folds of the ASE threshold as a function of the annealing temperature are demonstrated in **Figure 7**. The E_{th}^{ASE} of TrF2Py did not show significant changes from room temperature to 160 °C (1.2-fold to pristine films), while slightly increased E_{th}^{ASE} of TrFPy to 1.97-fold was noticed by annealing the pristine film at 160 °C. These results agreed well with the thermal and morphology stability results. The slightly higher loss of ASE for TrFPy before 160 °C may originate from crystallization that induces scattering, which would frustrate the

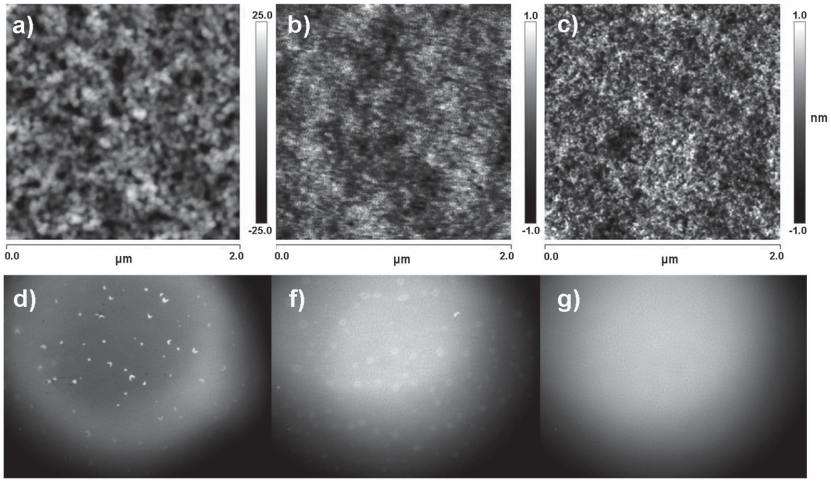

Figure 4. AFM images (top, as spun) and FOM images (annealed at 150 °C for 10 min in ambient condition) of a,d) TrPy, b,f) TrFPy, and c,g) TrF2Py on quartz. Scan size is 2 μm × 2 μm and scan rate is 1 Hz for AFM. The size of each FOM image corresponds to 88.8 μm × 67 μm, and all the FOM images were recorded at 550 nm.

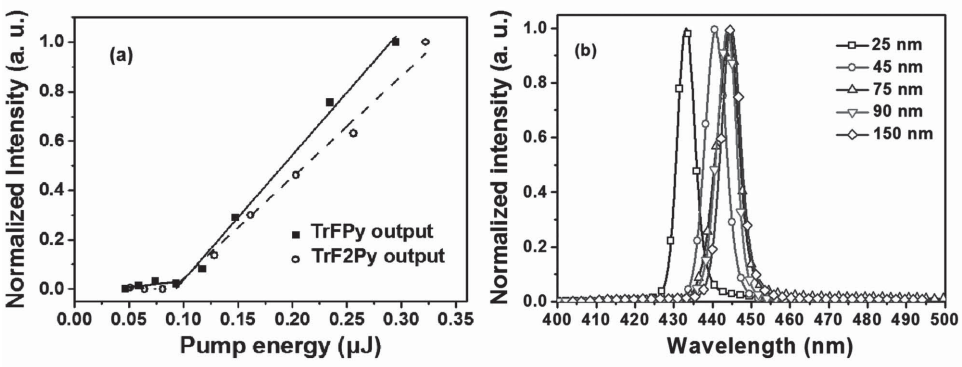

Figure 5. a) Normalized output intensity versus pump intensity for the TrFPy and TrF2Py films (90 nm); b) Normalized ASE spectra for TrF2Py films with various thicknesses: the emission peak at 433, 440, 443, 444, and 445 nm for TrF2Py films, corresponding to the thickness of 25, 45, 75, 90, and 150 nm, respectively.

required in-plane waveguide propagation. However, the E_{th}^{ASE} of TrF2Py films increased severely up to 17.6-fold relative to that of the pristine films when the annealing temperature approached 200 °C. In contrast, TrFPy showed relatively stable ASE performance for subsequent annealing temperature from 160 °C (1.97-fold relative to pristine films) to 200 °C (3.11-fold relative to pristine films). The ASE of TrFPy maintained good quality upon annealing even up to 250 °C with only 4.5-fold increment compared with that of the pristine films; while it was completely not detectable for TrF2Py. The results manifest that high thermal stability is helpful for improving the optical gain stability.

To further understand the origin for the different ASE behaviors of TrFPy and TrF2Py at high temperatures, the PL spectra of the same films after annealing are investigated and the results are shown in Figure S4 (Supporting Information). All the PL characteristics of both materials showed little variation by increasing the annealing temperature from 80 to 200 °C. However, for the TrF2Py film annealed at 250 °C, a weak green band (from 500 to 600 nm) appeared. In contrast, for TrFPy with a single fluorene bridge, the PL spectra remained almost the same with no obvious green emission band emerging even after annealing at 250 °C. The formation of the green band may result from both chemical and physical defects.[31] Since the films were annealed in an ambient atmosphere, the chemical degradation caused by the existence of oxygen and moisture in a rather high temperature (annealing at 250 °C) should have a significant impact on the optical properties. It is also suggested that long oligofluorene arms may favor intra-/inter-chain interactions between the arms.[12] Therefore, the only slightly enhanced green emission band for TrF2Py films after thermal annealing at high temperature (250 °C) may probably originate from the excimer formation of the stacked fluorene units, causing optical gain loss. [34]

3. Conclusion

In summary, we have presented the synthesis and characterization of a series of new trigonal starburst molecules comprising a truxene core and pyrene end-cappers with (TrFPy and TrF2Py) and without (TrPy) oligofluorene bridges. The π–π stacking of planar pyrene cappers were prevented by the introduction of fluorene bridges, resulting in the blueshifted PL spectra and enhanced PLQYs. In comparison to TrPy (35.7%), enhanced PLQYs of 56.2% for TrFPy and 60.1% for TrF2Py were achieved. The PL decay transients were reduced with the increase of fluorene bridge units. The incorporation of rigid pyrene cappers led to an enhancement of glass transition temperatures, which was beneficial for the morphology stability while pumped source

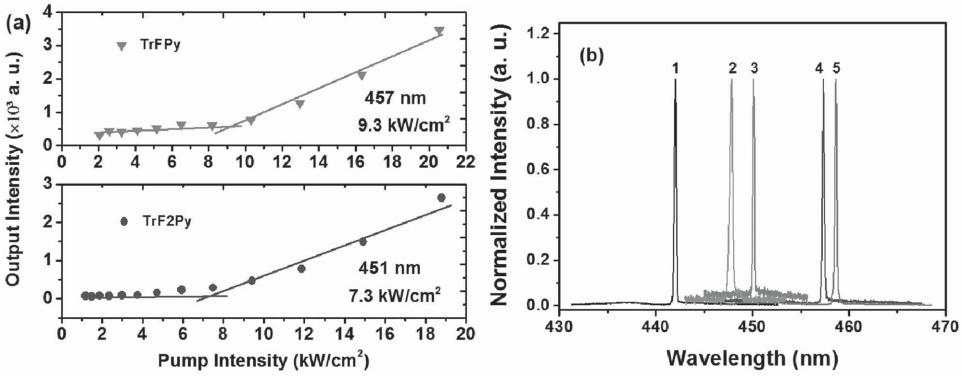

Figure 6. a) The output intensity as a function of the pump intensity for the TrFPy (top) and TrF2Py (bottom) lasers; b) The lasing spectra obtained by tuning the grating periods: 1, 3, and 5 for TrFPy films (thickness of 120 nm) with grating periods of 280, 290, and 300 nm respectively; 2 and 4 for TrF2Py films (thickness of 108 nm) with grating periods of 280 and 300 nm, respectively.

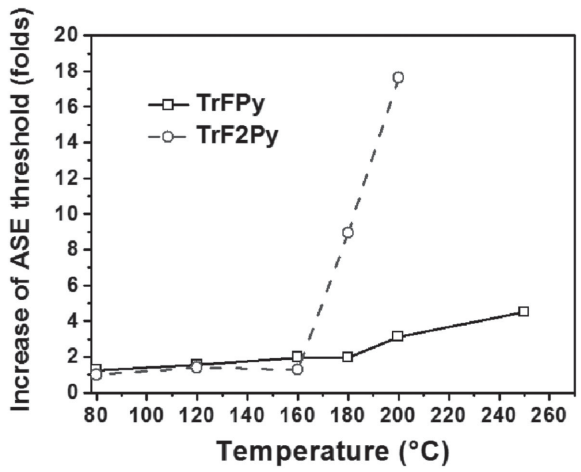

Figure 7. The increase of the ASE threshold as a function of the annealing temperature for 90 nm thick films (TrFPy and TrF2Py).

performing on them. The lowest ASE threshold for neat films was found to be 180 nJ pulse $^{-1}$ for TrFPy and 101 nJ pulse^{-1} for TrF2Py. A tunable optical window of 13 nm for TrF2Py (from 433to 445 nm) was achieved by controlling the thickness, and the ASE was even detectable for a thin film of 25 nm. 1D DFB lasing (50% fill factor, pumped source at 355 nm) demonstrated lasing threshold of 9.3 kW cm^{-2} and 7.3 kW cm^{-2} for TrFPy (at 457 nm) and TrF2Py lasers (at 451 nm), respectively. The lasing output wavelength could be fine-tuned by changing the periods of the gratings. In comparison to a slightly enhanced ASE threshold for TrFPy, the ASE for TrF2Py was found to be relatively robust against annealing in an ambient condition, which was less affected by heating up to 160 °C. The result was consistent with an absence of scattering-induced losses. However, the easier tendency of oxidation for TrF2Py in an ambient condition generated a significantly raised ASE threshold (17.6-fold relative to the as-spun films) when the annealing temperature was increased to 200 °C. In contrast, the TrFPy films showed excellent optical gain stability and the ASE can even be detectable after annealing at a very high temperature of 250 °C. These results suggest the utilization of pyrene as building blocks for exploring novel organic semiconductor gain media can effectively improve the thermal stability while maintain excellent lasing properties.

4. Experimental Section

Materials: All reagents and solvents, unless otherwise specified, were obtained from Aldrich, Acros, and TCI Chemical Co., and used as received. All manipulations involving air-sensitive reagents were performed under an atmosphere of dry nitrogen.

Synthesis of 1-(7-Bromo-9,9-dihexyl-9H-fluoren-2-yl)pyrene (4): A flask charged with 4,4,5,5-tetramethyl-2-(pyren-1-yl)-1,3,2-dioxaborolane (2) (500 mg, 1.52 mmol), 2,7-dibromo-9,9-dihexyl-9*H*-fluorene (3) (2.25 g, 4.56 mmol), $Pd(PPh_3)_4$ (53 mg, 0.04 mmol), and K_2CO_3 (20 mg) in toluene/water (2:1, 60 mL) was degassed for 15 min. After being refluxed for 24 h, it was cooled to room temperature and then extracted with $CHCl_3$ (25 mL × 3). The organic layer was washed with water, brine and dried with anhydrous $MgSO_4$. The solvent was removed and the residue was purified by silica gel column using hexane/CH_2Cl_2 (2:1) as eluent to afford 4 (516 mg, 55.2%) as a white powder. ^{1}H NMR (400 MHz, $CDCl_3$, δ): 8.29–8.16 (m, 4 H), 8.11 (*t*, *J* = 5.0 Hz, 2 H), 8.07–7.99 (m, 3 H), 7.86 (d, *J* = 7.7 Hz, 1 H), 7.68–7.58 (m, 3 H), 7.54–7.50 (m, 2 H), 2.10–1.93 (m, 4 H), 1.21–1.03 (m, 12 H), 0.84–0.75 (m, 10 H). ^{13}C NMR (100 MHz, $CDCl_3$, δ): 153.35, 150.53, 140.42, 139.93, 139.24, 138.10, 131.56, 131.01, 130.64, 130.11, 129.53, 128.63, 127.64, 127.49, 127.48, 126.29, 126.09, 125.36, 125.27, 125.21, 125.11, 124.98, 124.86, 124.69, 121.21, 121.18, 119.78, 55.60, 40.30, 31.56, 29.70, 23.91, 22.64, 14.08.

Synthesis of 2-(9,9-Dihexyl-7-(pyren-1-yl)-9H-fluoren-2-yl)-4,4,5,5-tetramethyl-1,3,2-dioxaborolane (5): A flask charged with 4 (400 mg, 0.33 mmol), bis(pinacolato)diborane (100 mg, 0.39 mmol), potassium acetate (121 mg, 1.24 mmol), $Pd(dppf)_2Cl_2$ (14 mg, 0.01 mmol), and 15 mL of anhydrous dioxane was degassed for 15 min. After the mixture was stirred at 95 °C for 12 h, it was cooled to room temperature and then poured into ice water (100 mL). The mixture was then extracted with $CHCl_3$, and the combined organic layers were dried over anhydrous $MgSO_4$. After the solvent was evaporated, the residue was purified by chromatography using silica gel (hexane: $CHCl_3$ = 2:1) to afford 5 (353 mg, 81.8%) as a white solid. ^{1}H NMR (400 MHz, $CDCl_3$, δ) : 8.29–8.16 (m, 4H), 8.15–8.08 (m, 3H), 8.07–8.00 (m, 2 H), 7.96–7.82 (m, 2 H), 7.84 (*d*, *J* = 2.8 Hz, 2 H), 7.66–7.61 (m, 2 H), 2.07 (*d*, *J* = 7.3 Hz, 4 H), 1.44 (s, 12 H), 1.21–1.07 (m, 12 H), 0.81 (*t*, *J* = 6.9 Hz, 10 H). ^{13}C NMR (100 MHz, $CDCl_3$, δ): 151.49, 150.29, 143.90, 140.40, 140.15, 138.33, 133.92, 131.55, 131.02, 130.57, 129.31, 128.96, 128.64, 127.69, 127.49, 127.42, 127.41, 126.06, 125.44, 125.40, 125.14, 125.10, 124.98, 124.82, 124.69, 120.13, 119.20, 83.79, 55.32, 40.26, 31.57, 29.74, 25.01, 23.88, 22.65, 14.11.

Synthesis of 1-(7′-Bromo-9,9,9′,9′-tetrahexyl-9H,9′H-[2,2′-bifluoren]-7-yl) pyrene (6): A flask charged with 5 (400 mg, 0.60 mmol), 2,7-dibromo-9,9-dihexyl-9*H*-fluorene (3) (0.88 g, 1.80 mmol), $Pd(PPh_3)_4$ (23 mg, 0.02 mmol), and K_2CO_3 (20 mg) in toluene/water (2:1, 60 mL) was degassed for 15 min. After being refluxed for 24 h, it was cooled to room temperature and then extracted with $CHCl_3$ (25 mL × 3). The organic layer was washed with water, brine and dried with anhydrous $MgSO_4$. The solvent was removed and the residue was purified by silica gel column using hexane/CH_2Cl_2 (2:1) as eluent to afford 6 (146 mg, 47.3%) as a white powder. ^{1}H NMR (400 MHz, $CDCl_3$, δ): 8.29–8.17 (m, 4 H), 8.14–8.08 (m, 3 H), 8.07–8.00 (m, 2 H), 7.93 (d, *J* = 8.1 Hz, 1 H), 7.89 (d, *J* = 7.8 Hz, 1 H), 7.77 (d, *J* = 7.9 Hz, 1 H), 7.72–7.60 (m, 7 H), 7.49 (d, *J* = 8.7 Hz, 2 H), 2.15–1.95 (m, 8 H), 1.12 (d, *J* = 16.1 Hz, 24 H), 0.94–0.75 (m, 20 H). ^{13}C NMR (100 MHz, $CDCl_3$, δ): 153.31, 151.93, 151.20, 151.18, 141.06, 140.49, 140.25, 139.99, 139.97, 139.90, 139.29, 138.36, 131.59, 131.06, 130.60, 130.05, 129.46, 128.68, 127.72, 127.50, 127.44, 127.42, 126.36, 126.27, 126.07, 125.46, 125.43, 125.16, 125.03, 124.83, 124.71, 121.55, 121.49, 121.12, 121.04, 120.14, 120.07, 119.77, 55.59, 55.42, 40.39, 40.33, 31.56, 31.50, 29.74, 29.67, 24.01, 23.79, 22.62, 22.61, 14.08, 14.05.

General Procedure for Synthesis of TrPy: The monomer 1 (229 mg, 0.815 mmol), 8 (200 mg, 0.163 mmol), TBAB (50 mg, 0.155 mmol) and $Pd(PPh_3)_4$ (62 mg) were placed in a 30 mL vessel. A mixture of 2 M K_2CO_3 aqueous solution (5 mL) and THF (15 mL) was added to the vessel. The mixture was then irradiated at 250 W for 30 min in microwave cavity. After the mixture was cooled to room temperature, it was extracted with $CHCl_3$ (25 mL × 3). The organic layer was washed with water, brine, and dried with anhydrous $MgSO_4$. The solvent was removed and the residue was purified by silica gel column using hexane/CH_2Cl_2 (2:1) as eluent to afford TrPy (213 mg, yield: 89.6%): ^{1}H NMR (400 MHz, $CDCl_3$, δ): 8.60 (d, *J* = 8.2 Hz, 3 H), 8.40–8.30 (m, 6 H), 8.25–8.00 (m, 21H), 7.80 (s, 3 H), 7.72 (d, *J* = 8.0 Hz, 3 H), 3.17 (d, *J* = 6.8 Hz, 6 H), 2.27 (d, *J* = 7.2 Hz, 6 H), 1.14–1.00 (m, 36 H), 0.82 (s, 12 H), 0.73 (t, *J* = 6.5 Hz, 18 H). ^{13}C NMR (100 MHz, $CDCl_3$, δ): 153.86, 145.50, 139.56, 139.23, 138.41, 138.24, 131.62, 131.11, 130.62, 128.72, 128.61, 127.77, 127.54, 127.50, 127.45, 126.08, 125.53, 125.22, 125.16, 125.09, 124.84, 124.77, 124.74, 124.71, 55.98, 37.06, 31.97, 31.65, 29.74, 29.70, 29.62, 29.40, 24.17, 22.73, 22.44, 14.16, 14.09. MALDI-TOF-MS (*m*/*z*): calcd for $C_{111}H_{114}$, exact mass: M^+ 1446.89; Found: 1446.5 (M^+), 1361.2 ([M-C_6H_{13}]$^+$).

TrFPy: The monomer 4 (501 mg, 0.815 mmol), 8 (200 mg, 0.163 mmol), TBAB (50 mg, 0.155 mmol), and $Pd(PPh_3)_4$ (62 mg) were placed in a 30 mL vessel. A mixture of 2 M K_2CO_3 aqueous solution (5 mL) and THF (15 mL) was added to the vessel. The mixture was then irradiated at 250 W for 30 min in microwave cavity. After the mixture was cooled to room temperature, it was extracted with $CHCl_3$ (25 mL × 3). The organic layer was washed with water, brine, and dried with anhydrous $MgSO_4$. The solvent was removed and the residue was purified by silica gel column using hexane/CH_2Cl_2 (2:1) as eluent to afford TrFPy (313 mg, yield: 78.3%). ^{1}H NMR (400 MHz, $CDCl_3$, δ): 8.58 (d, J = 8.4 Hz, 3 H), 8.35–7.95 (m, 33 H), 7.92–7.84 (m, 12 H), 7.69 (d, J = 6.8 Hz, 6 H), 3.21–3.06 (m, 6 H), 2.40–2.07 (m, 18 H), 1.26–1.16 (m, 36 H), 1.07–0.91 (m, 48 H), 0.86 (t, J = 6.7 Hz, 18 H), 0.69 (t, J = 6.9 Hz, 30 H). ^{13}C NMR (100 MHz, $CDCl_3$, δ): 173.39, 154.52, 151.95, 151.21, 145.26, 140.30, 140.20, 140.10, 139.93, 139.72, 139.51, 138.40, 138.21, 131.59, 131.06, 130.59, 129.47, 128.68, 127.75, 127.53, 127.46, 126.21, 126.09, 125.57, 125.46, 125.33, 125.15, 125.03, 124.84, 124.73, 121.35, 120.56, 120.21, 119.79, 55.93, 55.47, 40.54, 37.23, 31.65, 31.62, 30.36, 29.82, 29.75, 29.68, 24.15, 24.05, 22.69, 22.42, 14.13, 14.02. MALDI-TOF-MS (m/z): calcd for $C_{186}H_{210}$, exact mass: M^+ 2443.6; Found: 2443.7 (M^+), 2357.9 ($M\text{-}C_6H_{13}]^+$).

TrF2Py: The monomer 6 (772 mg, 0.815 mmol), 8 (200 mg, 0.163 mmol), TBAB (50 mg, 0.155 mmol), and $Pd(PPh_3)_4$ (62 mg) were placed in a 30 mL vessel. A mixture of 2 M K_2CO_3 aqueous solution (5 mL), and THF (15 mL) was added to the vessel. The mixture was then irradiated at 250 W for 30 min in microwave cavity. After the mixture was cooled to room temperature, it was extracted with $CHCl_3$ (25 mL × 3). The organic layer was washed with water, brine, and dried with anhydrous $MgSO_4$. The solvent was removed and the residue was purified by silica gel column using hexane/CH_2Cl_2 (1:1) as eluent to afford TrF2Py (401 mg, yield: 73.1%) (400 MHz, $CDCl_3$, δ): 8.57 (d, J = 7.8 Hz, 3 H), 8.33–8.04 (m, 27 H), 8.01–7.73 (m, 36 H), 7.69 (d, J = 6.9 Hz, 6 H), 3.22–3.04 (m, 6 H), 2.33-2.12 (m, 30 H), 1.24–1.18 (m, 60 H), 1.09–0.81 (m, 108 H), 0.69 (t, J = 6.9 Hz, 30 H). ^{13}C NMR (100 MHz, $CDCl_3$, δ): 154.50, 151.92, 151.87, 151.22, 145.25, 140.73, 140.57, 140.20, 140.17, 140.12, 140.05, 139.92, 139.68, 139.57, 138.40, 138.21, 131.59, 131.07, 130.59, 129.46, 128.68, 127.74, 127.52, 127.45, 126.28, 126.16, 126.08, 125.46, 125.32, 125.16, 125.03, 124.84, 124.72, 121.58, 121.38, 120.59, 120.15, 120.11, 120.08, 119.76. 55.92, 55.45, 55.43, 40.54, 40.44, 37.22, 31.63, 31.59, 31.55, 29.78, 29.75, 29.66, 24.13, 24.04, 23.94, 22.65, 22.41, 14.12, 14.10, 14.00. MALDI-TOF-MS (m/z): calcd for $C_{261}H_{306}$, exact mass: M^+ 3440.4; Found: 3440.8 (M^+), 3354.7 ($M\text{-}C_6H_{13}]^+$).

General Details: NMR spectra were recorded on a Bruker Ultra Shield Plus 400 MHz NMR (^{1}H: 400 MHz, ^{13}C: 100 MHz). The molecular weight of intermediates was measured by a Bruker matrix-assisted laser desorption/ionization time of flight mass spectrometry (MALDI-TOF MS) with CF_3COOAg and *trans*-2-[3-(4-tert-butylphenyl)-2-metheyl-2-propenylidene]malononitrile (DCTB) as the matrix. UV–vis spectra were measured with Shimadzu UV–vis–NIR spectrophotometer and photoluminescence spectra were recorded with Shimadzu Luminescence Spectrometer LS 50. AFM measurements of surface morphology were conducted on the Bruker ScanAsyst AFM in auto scan (AC) mode. Edinburgh instruments F900 Equipped using 375 nm excitation from a diode laser were used to obtain the PL decay times. For ASE measurements the samples were optically pumped with the pulsed (12 ns, 10 Hz) output from a Q-switched Nd:YAG laser pumped optical parametric amplifier (Spectron SL450) focused with a cylindrical lens to form a 4.10 mm × 0.44 mm stripe-shaped excitation area on the sample. The pulse energy incident on the sample was adjusted by the insertion of calibrated neutral density filters into the beam path. The ASE emission was monitored with a fiber-coupled spectrograph and a CCD detector from Oriel Instrument. For lasing, gratings with a 280, 290, and 300 nm period and the fill factor of 50% were used for turning the lasing wavelength and pumped source with the pulsed output (5 ns, 10 Hz) from Nd:YAG laser. The average modulation depth of the gratings was about 30 nm.

Fabrication of OLEDs: OLEDs were prepared on commercial glass slides coated with patterned indium tin oxide (ITO), which were cleaned in sequential ultrasonic baths using detergent solution, deionized water, acetone, and isopropanol. A thin layer of poly(styrene sulfonic acid)-doped-poly(3,4-ethylenedioxy thiophene) (PEDOT:PSS) (40 nm) was spin-coated onto ITO substrate, which was then treated with O_3 for 0.5 h. After baking at 120 °C for 0.5 h in an oven installed inside a glovebox with argon, a thin layer (80 nm) of TrFPy or TrF2Py were spin-coated on top of the treated ITO substrate from its toluene solution (18 mg mL^{-1}) at 1000 rpm. At last, a thin layer of LiF (1.2 nm) and Al (80 nm) was deposited by thermal evaporation through a shadow mask in a high vacuum chamber under a pressure of 10^{-6} Torr.

Supporting Information

Supporting Information is available from the Wiley Online Library or from the author.

Acknowledgements

This study was supported by the National Key Basic Research Program of China (973 Program, Grant No. 2014CB648300), the National Natural Science Foundation of China (Grant Nos. 21422402, 20904024, 51173081, and 61136003), the Natural Science Foundation of Jiangsu Province (Grant Nos. BM2012010, BK20140060, and BK20130037), Program for New Century Excellent Talents in University (NCET-13-0872), Specialized Research Fund for the Doctoral Program of Higher Education (Grant No. 20133223110008), the Ministry of Education of China (IRT1148), the Synergetic Innovation Center for Organic Electronics and Information Displays, the Priority Academic Program Development of Jiangsu Higher Education Institutions (PAPD), the Six Talent Plan (Grant No. 2012XCL035) and the Qing Lan Project of Jiangsu Province.

Received: April 3, 2015
Revised: May 19, 2015
Published online: June 18, 2015

[1] C. Grivas, M. Pollnau, *Laser Photonics Rev.* **2012**, *6*, 419.
[2] S. R. Forrest, *Nature* **2004**, *428*, 911.
[3] G. D. Scholes, G. Rumbles, *Nat. Mater.* **2006**, *5*, 683.
[4] I. D. W. Samuel, G. A. Turnbull, *Chem. Rev.* **2007**, *107*, 1272.
[5] D. Amarasinghe, A. Ruseckas, A. E. Vasdekis, G. A. Turnbull, I. D. W. Samuel, *Adv. Mater.* **2009**, *21*, 107.
[6] B. K. Yap, R. Xia, M. Campoy-Quiles, P. N. Stavrinou, D. D. C. Bradley, *Nat. Mater.* **2008**, *7*, 376.
[7] E. B. Namdas, M. Tong, P. Ledochowitsch, S. R. Mednick, J. D. Yuen, D. Moses, A. J. Heeger, *Adv. Mater.* **2009**, *21*, 799.
[8] X.-F. Jiang, Y.-F. Xiao, C.-L. Zou, L. He, C.-H. Dong, B.-B. Li, Y. Li, F.-W. Sun, L. Yang, Q. Gong, *Adv. Mater.* **2012**, *24*, 260.
[9] M. M. Mróz, G. Sforazzini, Y. Zhong, K. S. Wong, H. L. Anderson, G. Lanzani, J. Cabanillas-Gonzalez, *Adv. Mater.* **2013**, *25*, 4347.
[10] W. Y. Lai, R. Zhu, Q.-L. Fan, L.-T. Hou, Y. Cao, W. Huang, *Macromolecules* **2006**, *39*, 3707.
[11] R. Xia, W. Y. Lai, P. A. Levermore, W. Huang, D. D. C. Bradley, *Adv. Funct. Mater.* **2009**, *19*, 2844.
[12] W. Y. Lai, R. Xia, Q.-Y. He, P. A. Levermore, W. Huang, D. D. C. Bradley, *Adv. Mater.* **2009**, *21*, 355.
[13] W.-Y Lai, R. Xia, D. D. C. Bradley, W. Huang, *Chem. Eur. J.* **2010**, *16*, 8471.
[14] W.-Y. Lai, Q.-Q. Chen, Q.-Y. He, Q.-L. Fan, W. Huang, *Chem. Comm.* **2006**, *18*, 1959.

[15] M. Sims, K. Zheng, M. Campoy-Quiles, R. Xia, P. N. Stavrinou, D. D. C. Bradley, P. Etchegoin, *J. Phys. Condens. Matter* **2005**, *17*, 6307.
[16] T. M. Figueira-Duarte, K. Müllen, *Chem. Rev.* **2011**, *111*, 7260.
[17] F. Liu, W. Y. Lai, C. Tang, H. B. Wu, Q. Q. Chen, B. Peng, W. Wei, W. Huang, Y. Cao, *Macromol. Rapid Commun.* **2008**, *29*, 659.
[18] L. Zöphel, D. Beckmann, V. Enkelmann, D. Chercka, R. Rieger, K. Müllen, *Chem. Commun.* **2011**, *47*, 6960.
[19] J. C. Xiao, S. W. Liu, Y. Liu, L. Ji, X. W. Liu, H. Zhang, X. W. Sun, Q. C. Zhang, *Chem. Asian J.* **2012**, *7*, 561.
[20] J. C. Xiao, C. D. Malliakas, Y. Liu, F. Zhou, G. Li, H. B. Su, M. G. Kanatzidis, F. Wudl, Q. C. Zhang, *Chem. Asian J.* **2012**, *7*, 672.
[21] J. B. Li, P. Z. Li, J. S. Wu, J. K. Gao, W.-W. Xiong, G. D. Zhang, Y. L. Zhao, Q. C. Zhang, *J. Org. Chem.* **2014**, *79*, 4438.
[22] P.-Y. Gu, Y. B. Zhao, J.-H. He, J. Zhang, C. Y. Wang, Q.-F. Xu, J.-M. Lu, X. W. Sun, Q. C. Zhang, *J. Org. Chem.* **2015**, *80*, 3030.
[23] K. A. Zachariasse, *Trends Photochem. Photobiol.* **1994**, *3*, 211.
[24] T. M. Figueira-Duarte, P. G. D. Rosso, R. Trattnig, S. Sax, E. J. W. List, K. Müllen, *Adv. Mater.* **2009**, *22*, 990.
[25] F. Liu, L. H. Xie, C. Tang, J. Liang, Q. Q. Chen, B. Peng, W. Wei, Y. Cao, W. Huang, *Org. Lett.* **2009**, *11*, 3850.
[26] C. Tang, F. Liu, Y. J. Xia, L. H. Xie, A. Wei, S. B. Li, Q. L. Fan, W. Huang, *J. Mater. Chem.* **2006**, *16*, 4074.
[27] C. Tang, F. Liu, Y. J. Xia, J. Lin, L. H. Xie, G. Y. Zhong, Q. L. Fan, W. Huang, *Org. Electron.* **2006**, *7*, 155.
[28] Z. Q. Liang, Z. Z. Chu, J. X. Yang, C. X. Yuan, X. T. Tao, D. C. Zou, *Synth. Met.* **2011**, *161*, 1691.
[29] Z. J. Zhao, J. H. Li, X. P. Chen, X. M. Wang, P. Lu, Y. Yang, *J. Org. Chem.* **2009**, *74*, 383.
[30] R. R. Reghu, J. V. Grazulevicius, J. Simokaitiene, A. Miasojedovas, K. Kazlauskas, S. Jursenas, P. Data, K. Karon, M. Lapkowski, V. Gaidelis, V. Jankauskas, *J. Phys. Chem. C* **2012**, *116*, 15878.
[31] G. Zeng , W.-L. Yu, S.-J. Chua, W. Huang, *Macromolecules* **2002**, *35*, 6907.
[32] A. L. Kanibolotsky, R. Berridge, P. J. Skabara, I. F. Perepichka, D. D. C. Bradley, M. Koeberg, *J. Am. Chem. Soc.* **2004**, *126*, 13695.
[33] F. Laquai, P. E. Keivanidis, S. Baluschev, J. Jacob, K. Müllen, G. Wegner, *Appl. Phys. Lett.* **2005**, *87*, 261917.
[34] J. Kang, J. Jo, Y. Jo, S. Y. Lee, P. E. Keivanidis, G. Wegner, D. Y. Yoon, *Polymer* **2008**, *49*, 5700.